APPENDICES: Sulfate sulfur isotopes and major ion chemistry reveal that pyrite oxidation counteracts CO_2 drawdown from silicate weathering in the Langtang-Trisuli-Narayani River system, Nepal Himalaya

P.C. Kemeny[a*], G.I. Lopez[a], N. F. Dalleska[a], M. Torres[b], A. Burke[c], M.P. Bhatt[d], A.J. West[e], J. Hartmann[f], J.F. Adkins[a]

[a] Division of Geological and Planetary Sciences, California Institute of Technology, Pasadena, California, USA
[b] Department of Earth, Environmental, and Planetary Sciences, Rice University, Houston, Texas
[c] School of Earth and Environmental Sciences, University of St Andrews, St Andrews, UK
[d] Department of Physical and Environmental Sciences, Concord University, Athens, WV, USA
[e] Department of Earth Science, University of Southern California, Los Angeles, California, USA
[f] Institute for Geology, Universität Hamburg, Bundesstrasse, Hamburg, Germany
[*]Corresponding author: pkemeny@caltech.edu, preston.kemeny@gmail.com

Contents

Appendix 1: Ion Chromatography

Initial MC-ICP-MS measurements of $\delta^{34}S_{SO4}$ revealed lower S abundances than expected based on the [SO_4^{2-}] values reported in Bhatt et al. (2018). Subsequent ion chromatography (IC) measurements at Caltech of [Ca^{2+}], [Mg^{2+}], [Na^{+}], [K^{+}], [Cl^{-}], and [SO_4^{2-}] revealed systematic differences from the published values, with trends related to the month of sample collection (Fig. S1). Two potential causes of the discrepancy are analytical uncertainty and changes in sample chemistry due to storage artifacts.

1.1 Analytical uncertainty

To ascertain if the discrepancy in measured ion concentrations is attributable to experimental uncertainty, we quantified precision through replicate analysis of external reference materials and river water samples. For reference materials, we used *Environment and Climate Change Canada* certified materials MAURI-09 (lot 0316) and CRANBERRY-05 (lot 0815). A subset of references and samples were also measured after addition of variable quantities of HNO_3^-; we report precision both for all determinations of major ion chemistry (Table S1, row tops) and for determinations on only solutions without added HNO_3^- (Table S1, bottom rows). When calculated as the mean of the relative standard deviation of measurements on the two reference materials, we find the following precisions across all determinations of major ion concentration (2σ): [Ca^{2+}]: 8.4%, [Mg^{2+}]: 5.7%, [Na^{+}]: 1.6%, [K^{+}]: 3.1%, [Cl^{-}]: 2.8%, [SO_4^{2-}]: 2.7%. When quantified as the relative standard deviation of replicate sample measurements, we find the following measurement precisions across all determinations of major ion concentration (2σ): [Ca^{2+}]: 3.6%, [Mg^{2+}]: 3.7%, [Na^{+}]: 1.1%, [K^{+}]: 1.4%, [Cl^{-}]: 2.8%, [SO_4^{2-}]: 2.5% (Table S1). Overall, we conservatively quantify the 2σ precision of any given ion measurement to be <12%, which represents the least-reproducible ion (Ca^{2+}) in

the least-reproducible solution, when also including measurements with added HNO_3^- (Table S1). When measurements are only considered on references and samples without added HNO_3^-, we conservatively quantify the 2σ precision of any given ion measurement to be <7%. Given the large differences between Caltech measurement and those of Bhatt et al. (2018) (Fig. S1), low analytical precision is unable to explain the discrepancy.

For MAURI-09 the fractional offset between the mean measured value and the mean certified values were: $[Ca^{2+}]$: 9.8%; $[Mg^{2+}]$: 4.8%; $[Na^+]$: 2.2%; $[K^+]$: 5.2%; $[Cl^-]$: 2.1%; $[SO_4^{2-}]$: 2.0%. For CRANBERRY-05 the fractional offset between the mean measured value and the mean certified values were: $[Ca^{2+}]$: 4.6%; $[Mg^{2+}]$: 3.5%; $[K^+]$: 3.7%; $[SO_4^{2-}]$: 3.0%, with $[Na^+]$ and $[Cl^-]$ outside of the calibration range. Despite the relatively high difference for the measured and reported concentration of $[Ca^{2+}]$ in MAURI-09, we accept our $[Ca^{2+}]$ determinations because (i) the measured $[Ca^{2+}]$ is close to being within the stated 2σ uncertainty window of the certified value, (ii) the same calibration standards generated a reasonable match with the reported $[Ca^{2+}]$ of CRANBERRY-05, (iii) our $[Ca^{2+}]$ measurements match expected values for a different set of standards prepared by a different analyst and made from a separate Ca^{2+} stock solution, and (iv) the consistency of our measurements with all other reported ion systems argues against mistakes during sample handling or data processing.

1.2 Artifacts of sample storage

The samples measured in this study were collected in 2011 in a variety of bottles. Except for the fact that samples from a given month tend to have been collected in the same type of container, the trendlines in Fig. S1 are not associated with the type of sample bottle. After collection, only a

minimal number of primary liquids were transferred into secondary containers. The samples were stored refrigerated without acidification in Germany until their shipment to California in early 2018, where they were again stored refrigerated and unacidified.

During storage ions could have either adsorbed to the sides of the sample bottles, precipitated as solids (Jacobson et al., 2002), or been concentrated through evaporation. In the first two cases, we expect the Caltech measurements of ion concentration to be lower than those reported in Bhatt et al. (2018). However, for certain ions and time periods, the Caltech measurement is significantly higher than that of Bhatt et al. (2018). Moreover, no solids are visually identifiable in the sample containers, and precipitation of a carbonate phase would be unlikely to explain the discrepancy of ions such as [Cl^-] and [K^+]. To test if the discrepancy is attributable to artifacts of sample storage, two subsets of ten samples each were acidified with nitric acid, one set to ~0.1% and the second set to ~0.2%. Measurements of [Ca^{2+}], [Mg^{2+}], [Na^+], and [K^+] before and after acidification were very similar for both sets of samples, typically within 5% (Fig. S2). There is a general tendency for measured [Ca^{2+}] and [Mg^{2+}] to be approximately 2.5% to 3.5% lower in acidified samples than in unacidified samples, which is opposite to the shift expected if cations were attached to the walls of the sample bottles or precipitated as an acid-soluble phase. Notably, measurement of [Ca^{2+}] in acidified MAURI-09 and calibrated with acidified standards was significantly more consistent with the reported value than measurement of [Ca^{2+}] in unacidified MAURI-09 calibrated with unacidified standards. Given the similarity of cation measurements in samples before and after acidification, we do not believe that either ion attachment to the walls of sample containers or precipitation of solids can explain the discrepancy between the Caltech measurements and those of Bhatt et al. (2018).

Evaporation of samples during storage is expected to increase the concentration of each major ion in solution by the same proportion. Contrary to this expectation, the sign and magnitude of discrepancy between the Caltech measurements and those of Bhatt et al. (2018) differ across ion systems within the same samples. For example, the two sets of measurements of $[Mg^{2+}]$ in samples from April are much more consistent than the two sets of measurements of $[Na^{+}]$ in the same sample bottles (Fig. S1). This indicates that evaporation of samples during storage is unable to explain the discrepancy between the Caltech measurements and those of Bhatt et al. (2018).

1.3 Comparison with prior measurements

The 2011 sampling campaign is one of several in the Lirung Glacier catchment and the Trisuli River at Betrawati. Samples from the Lirung Glacier catchment were previously analyzed in Bhatt et al. (2000) and Bhatt et al. (2009), and the major ion composition of waters from the Trisuli River at Betrawati were previously reported in Galy and France-Lanord (1999) and Bhatt et al. (2009). For the Lirung samples, the Caltech measurements of $[Cl^{-}]$ and Cl^{-}/Σ^{+} are higher than previous observations (Fig. S3a, b). Although the fractional difference in $[Cl^{-}]$ is large, the change translates to only a few percent of Cl^{-}/Σ^{+}. For the Trisuli River at Betrawati, the major ion composition of our samples is largely similar to that reported in Galy and France-Lanord (1999).

1.4 Re-evaluation of the Bhatt et al. (2018) measurements

A subset of the chromatographic measurements underlying the reported values in Bhatt et al. (2018) were recovered and reprocessed. In particular, the original measurements of $[Na^{+}]$, $[SO_4^{2-}]$, and $[Ca^{2+}]$ for several samples from January, March, and November were re-evaluated and

compared with the new Caltech measurements. For [Na^+], the updated analysis brought samples from January, March, and November into much stronger agreement, although several samples from March still remain >10% discrepant. For [SO_4^{2-}] in November samples, the updated values brought most of the measured concentrations within 10% agreement. For [SO_4^{2-}] in January samples, the updated values increased the difference in measured concentrations beyond 10%. No reprocessing of the original [Ca^{2+}] data was required.

1.5 Summary of major ion discrepancy

If the difference in the Caltech and Bhatt et al. (2018) measurements were due to random errors, the Caltech measurements would scatter around a 1:1 line with those reported in Bhatt et al. (2018). Rather, the data show clear trends correlated with the month of sample collection (Fig. S1). If the discrepancy were due to a constant accuracy offset, the measurements of a given ion at Caltech should be systematically lower or higher than those published previously. However, in some months the Caltech measurements show higher ion concentrations, while in other months the measurements of Bhatt et al. (2018) are higher. Acidification testing rules out storage artifacts, and the changing magnitude of discrepancy across ion systems argues against evaporation during sample storage. To promote comparison between our $\delta^{34}S_{SO4}$ measurements and ionic weathering products, we remeasured the major ion chemistry in all samples used for sulfur isotope analysis. In the main text of this article, we report the major ion chemistry measured at Caltech.

	Ion	MAURI-09 2σ, RSD	CRANBERRY-05 2σ, RSD	SAMPLES, mean 2σ RSD
Solutions with or without addition of HNO_3^-	Ca^{2+}	11.6% (n=16)	5.2% (n=7)	3.6% (n=42)
	Mg^2	7.9% (n=16)	3.5% (n=7)	3.7% (n=41)
	Na^+	1.6% (n=16)	-	1.1% (n=41)
	K^+	3.4% (n=16)	2.8% (n=7)	1.4% (n=42)
	Cl^-	2.8% (n=73)	-	2.8% (n=44)
	SO_4^{2-}	2.7% (n=73)	2.8% (n=15)	2.5% (n=54)
Solutions without addition of HNO_3^-	Ca^{2+}	6.8% (n=14)	2.4% (n=5)	2.2% (n=26)
	Mg^2	4.8% (n=14)	2.1% (n=5)	2.3% (n=25)
	Na^+	1.6% (n=14)	-	1.2% (n=25)
	K^+	2.7% (n=14)	2.3% (n=5)	1.0% (n=26)

Table S1: Precision of Caltech IC measurements (2σ, relative standard deviation). For MAURI-09 and CRANBERRY-05 the value n in parentheses refers to the number of unique determinations, while for samples the value n in parentheses refers to the number of samples measured twice or more. Precision is given in the top section of the table for all determinations of major ion concentrations, including references and samples with added HNO_3, and in the bottom section for determinations of major ion chemistry in only un-acidified standard and references.

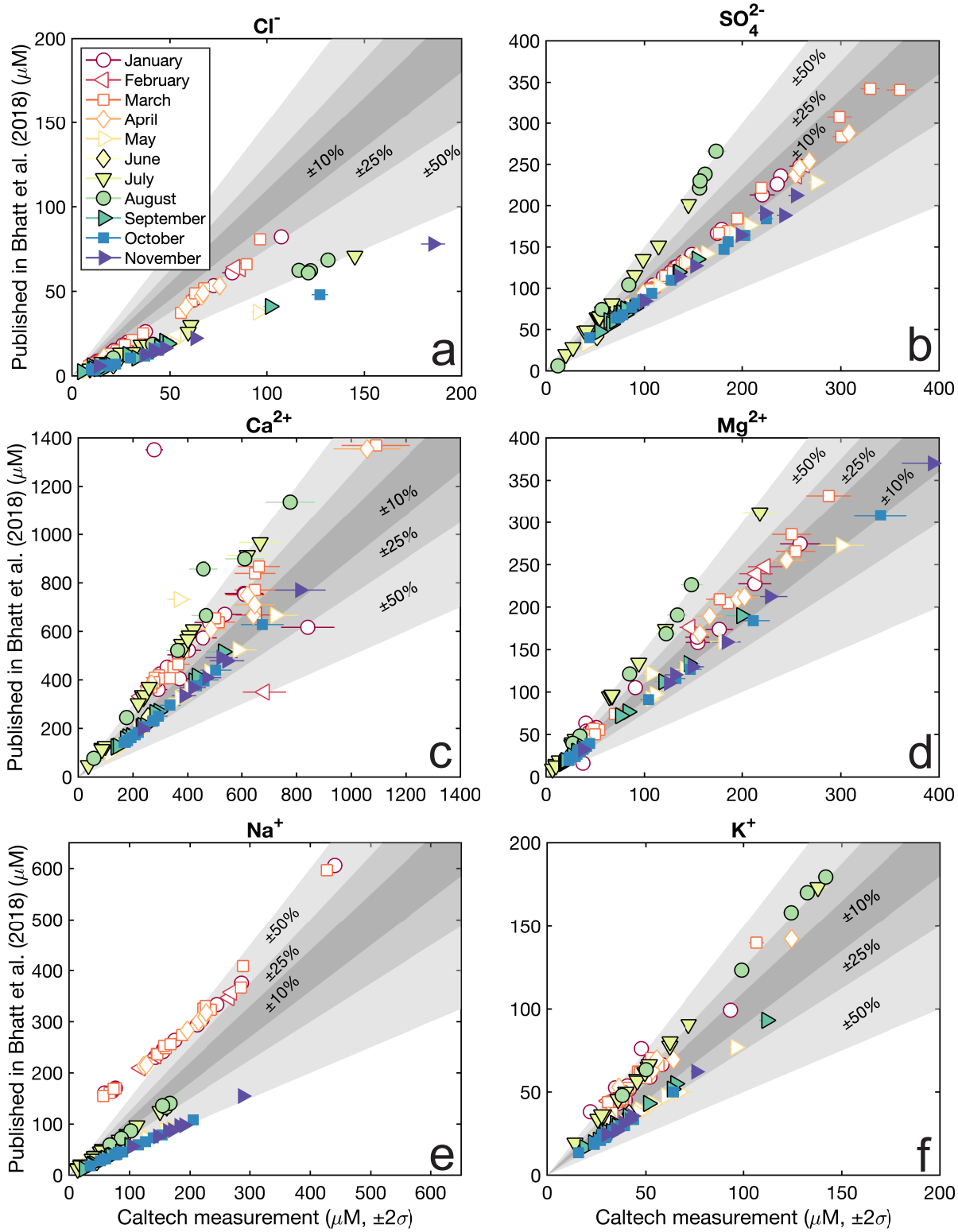

Fig. S1: Comparison of (a) [Cl^-], (b) [SO_4^{2-}], (c) [Ca^{2+}], (d) [Mg^{2+}], (e) [Na^+], and (f) [K^+] in sample bottles measured at Caltech and previously published in Bhatt et al. (2018). Shaded regions show ±10%, ±25%, and ±50% from mutual agreement. Systematic offsets group by month of sample collection.

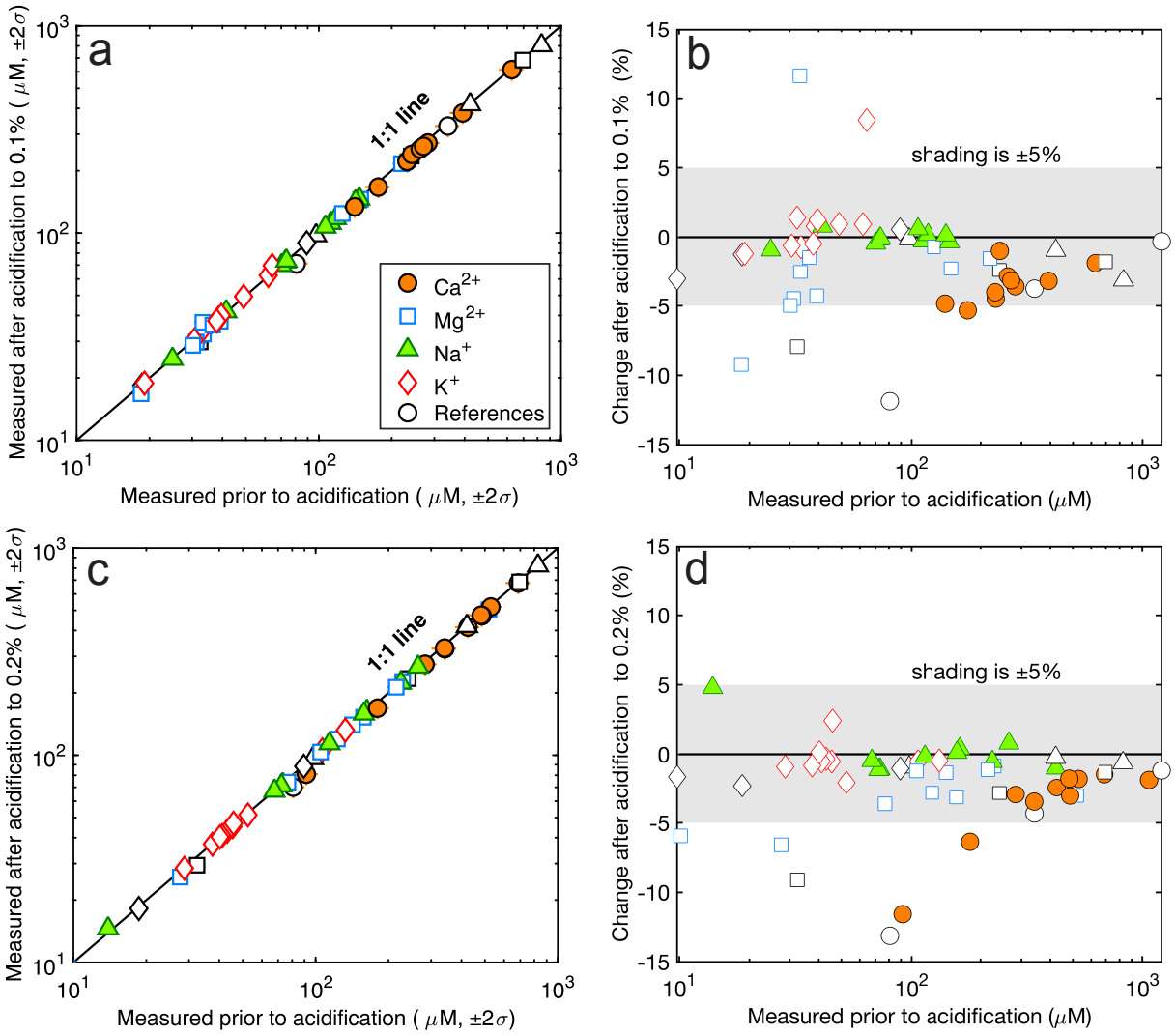

Fig. S2: $[Ca^{2+}]$, $[Mg^{2+}]$, $[Na^{+}]$, and $[K^{+}]$ in river samples before and after acidification to approximately (a, b) 0.1% and (c, d) 0.2% with high-purity HNO_3. (b, d) Proportional change following acidification is mostly within 5%.

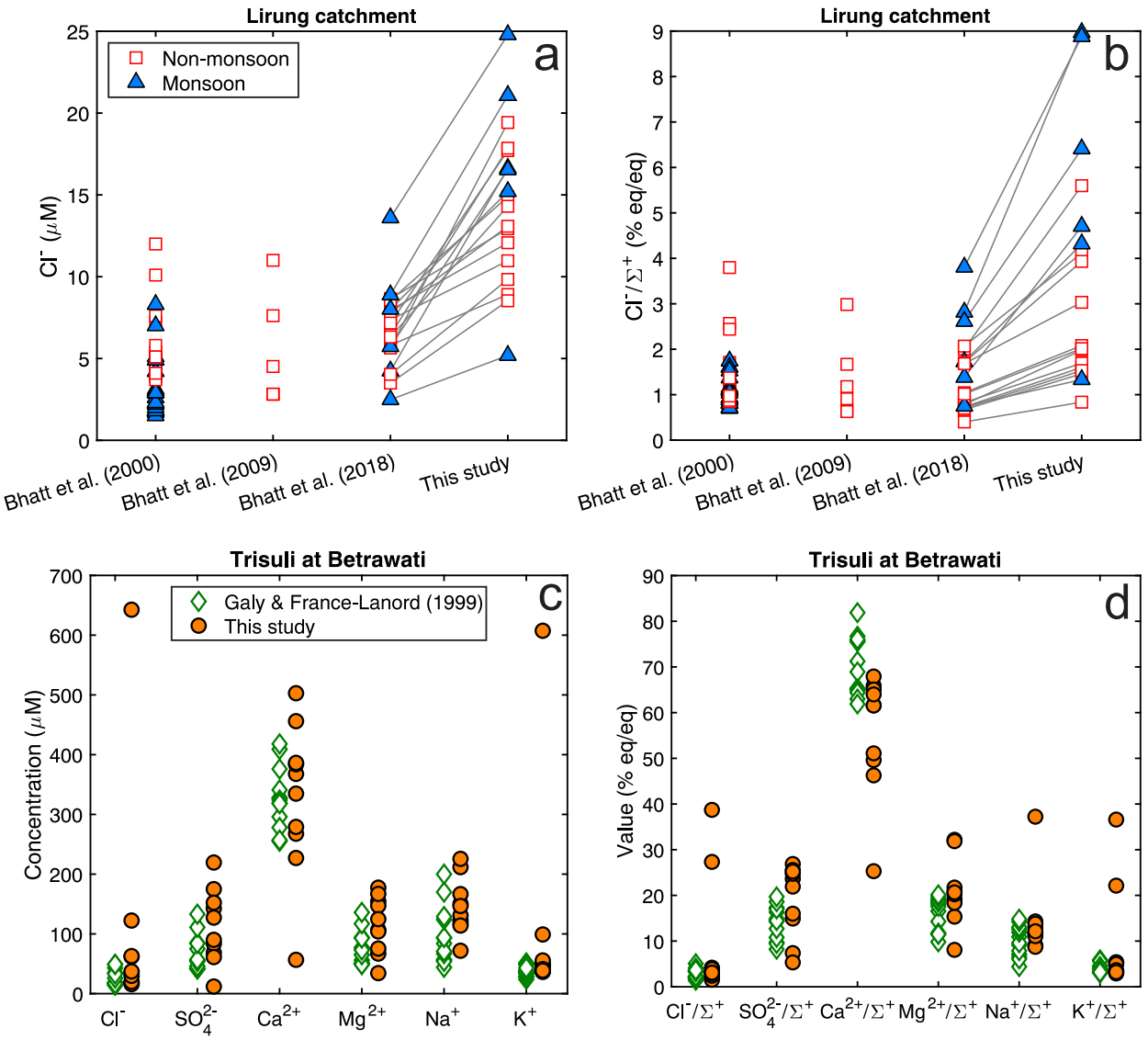

Fig. S3: (a) [Cl^-] and (b) Cl^-/Σ^+ for samples from the Lirung Glacier catchment reported in Bhatt et al. (2000, 2009, 2018) and in this study. Samples from Bhatt et al. (2009, 2018) and this study are those from LNS-13, LNS-14, and LNS-15. Grey lines link the measurement of Bhatt et al. (2018) to the measurement of the same sample in this study. With some exceptions, these two measurements are on liquid taken from the same original sample bottle. (c) [Cl^-], [SO_4^{2-}], [Ca^{2+}], [Mg^{2+}], [Na^+], and [K^+] and (d) ratios relative to the sum of cations ([Ca^{2+}] + [Mg^{2+}] + [Na^+] + [K^+] in units of charge equivalents) for samples from LNS-4 and from the Trisuli River sampled at Betrawati (Galy and France-Lanord, 1999). Measurements are comparable to those previously reported at Betrawati, but with several outliers to higher Cl^-/Σ^+, higher K^+/Σ^+, and lower Ca^{2+}/Σ^+.

Appendix 2: Inversion end-members

2.1: Carbonate end-members

In forward models, the contribution of carbonate lithologies to river dissolved load is often found by differencing after attributing portions of the river dissolved load to cyclic salts and silicate lithologies (Galy and France-Lanord 1999; Quade et al., 2003). In contrast, inversion modeling requires defining parameter ranges for the composition of carbonate end-members. Here we use stoichiometric calcite and dolomite as two carbonate end-members with $Na^+/\Sigma^+ = K^+/\Sigma^+ = 0$. This choice is enabled by our normalization to Σ^+, rather than Na^+, which allows the carbonate end-members to not provide Na^+ to river water. In prior work, Gaillardet et al. (1999) used a Ca^{2+}/Na^+ of 50 and Mg^{2+}/Na^+ of 10, while Burke et al. (2018) followed the Congo study of Négrel et al. (1993) to use a carbonate Ca^{2+}/Na^+ of 60±30 and Mg^{2+}/Na^+ of 30±15.

2.2: Silicate end-members

Coherently changing K^+/Na^+ ratios (Fig. 3b) motivates the use of two silicate end-members, which we call 'silicate' and 'biotite'. We take the silicate and biotite end-members to have Ca^{2+}/Σ^+ of 0.15±0.05 and Mg^{2+}/Σ^+ of 0.35±0.10, informed by XRF measurements of HHC bedrock (France-Lanord and Derry, 1997). The Na^+/Σ^+ and K^+/Σ^+ ratios of the two end-members are 0.1±0.1 and 0.4±0.1 (Table 1).

Quade et al. (2003) report a silicate end-member $Ca^{2+}/Na^+ = 0.41±0.18$ based on a subset of Himalayan rivers thought to be draining only silicate minerals, similar to the value of 0.45 derived from suspended sediments in the Marsyandi (Wolf-Boenisch et al., 2009). However, both values are higher than the range of 0.18-0.30 reported in Galy and France-Lanord (1999) for Himalayan

silicates and are higher than the value 0.35±0.15 used to invert global river observations (Gaillardet et al., 1999). Conversely, these values are all lower than the Ca^{2+}/Na^{+} of 0.7±0.3 reported in Krishnaswami and Singh (1998). The Ca^{2+}/Na^{+} ratio of silicates may also change across lithostratigraphic units; according to Dalai et al. (2002), Krishnaswami et al. (1999) indicate a Ca^{2+}/Na^{+} ratio of 0.46±0.28 for granite and gneiss in the LH, but 0.32±0.29 for the HHC.

Quade et al. (2003) report a silicate Mg^{2+}/Na^{+} ratio of 0.24±0.1, which is quoted as a likely maximum due to detection limitations, and which is almost identical to the value of 0.24±0.12 inferred from the global compilation of Gaillardet et al. (1999). Conversely, Dalai et al. (2002) reports Mg^{2+}/Na^{+} from the Yamuna River system of 0.65±0.45 for the LH and 0.31±0.28 for the HHC. Spanning this entire range, values of Mg^{2+}/Na^{+} in suspended sediments from the Marsyandi River range from 0.11-1.30 (Wolff-Boenisch et al., 2009).

2.3 Evaporite end-member

Sarin and Krishnaswami (1984) raised the prospect that evaporites may exist in the central Nepal Himalaya based on the observation of gypsum associated with the Kumaun Himalya (Valdiya, 1980). Subsequently, the presence of western evaporites was confirmed through direct observations of gypsum and halite near the Main Boundary Trust in North India (Singh and Singh, 2010). While general thinking holds that evaporites are unlikely to be a major influence in the Narayani River catchment, they may still be important locally. For example, Fort (1996) cites a study by Tshering and Bhandari (1973) ostensibly showing the existence of evaporitic layers in the Thakkhola-Mustang Valley. Citing Bordet et al. (1971), Tipper et al. (2006) writes that no evaporites have been identified in TSS sediment near the Marsyandi headwaters. Turchyn et al.

(2013) provided support for this claim by not recovering a clear correlation between [Cl^-] and $\delta^{34}S_{SO4}$. If present, evaporite $\delta^{34}S$ is expected to reflect the range of Phanerozoic evaporites and thus fall between 10‰ and 30‰ (Claypool et al., 1980). Given the lack of direct observation of evaporites along the Langtang-Trisuli-Narayani River system, we do not include an evaporite end-member in our primary inversion (see Appendix 4 for results from an inversion including an evaporite end-member).

2.4. Geothermal spring end-member

The dissolved chemistry of Himalayan geothermal springs varies over multiple orders of magnitude and exhibits large spatial gradients (Fig. S4; Evans et al., 2001, 2004; Becker et al., 2008). In part, the chemical variability is attributable to mixing between a geothermal end-member and river waters influenced by weathering. Ion ratios in spring waters often resemble seawater, although this observation could reflect the excess of sampling from the Marsyandi River relative to springs from elsewhere in the Narayani River system. In the space of Ca^{2+}/Σ^+ against Na^+/Σ^+ (Fig. S4a), the data appear consistent with mixing between an end-member resembling seawater and another end-member resembling river water (Fig. S4a). However, this trend breaks down when considering Na^+/Cl^- and K^+/Cl^- (Fig. S4e).

Previously, Bickle et al. (2005) estimated the chemistry of a spring end-member by selecting 11 springs from Evans et al. (2001) with $Na^+/Cl^- < 1.2$. This choice was influenced by initial work in the Marsyandi River that found springs tend to be highly enriched in Cl^-, suggestive of an influence from deep evaporites (Evans et al., 2001). Although subsequent work showed that the dominant anion in Himalayan geothermal springs is HCO_3^-, with Cl^- thought to derive from metamorphism,

a potential role for evaporite weathering at depth in the Marsyandi is still supported by a single hot spring $\delta^{34}S_{SO4}$ measurement of +12.4‰ (Turchyn et al., 2013). While the criteria of Bickle et al. (2005) thus may be appropriate for the Marsyandi, it does not necessary reflect the chemistry of geothermal springs in the Langtang-Trisuli-Narayani River system.

Springs are found in the general vicinity of LNS-5, LNS-6, and LNS-7 on the Langtang River upstream of the junction at Syabru Besi and along the Bhote Kosi (Evans et al., 2004, 2008; Becker et al., 2008). These springs have Cl^-/Na^+ ratios between 0.3% and 9.8%. In contrast, springs near the Marsyandi have Cl^-/Na^+ ratios close to or slightly exceeding 100%, which represent an exception to the general observation that HCO_3^- dominates the anion budgets of Himalayan hot springs (Evans et al., 2004). Overall, the data show that geothermal springs along the Langtang-Trisuli have significantly lower Na^+/Cl^- ratios than seawater and springs from the Marsyandi River (Fig. S4c). In all samples from this study, correcting for 100% of $[Cl^-]$, even using the highest Cl^-/Na^+ ratio of the relevant springs, would remove >100% of $[Na^+]$. Attributing 10% of the river Cl^- budget to springs would, on average, source 43% of dissolved $[Na^+]$. Although this magnitude of input is potentially acceptable, the remaining 90% of Cl^- in solution would still require an alternative explanation. Given the large chemical difference between springs and river samples, we do not anticipate significant inputs from springs and do not include a spring end-member in our primary analysis (see Appendix 4 for results from an inversion model including springs).

If springs do contribute Cl^- to our samples, we expect only a moderate influence on river $\delta^{34}S_{SO4}$. The SO_4^{2-}/Cl^- of the relevant springs ranges from 0.4 to 26, and a contribution of 10% of river $[Cl^-]$ would entail median contributions of 0.5% to 33% of river $[SO_4^{2-}]$. Taking a spring $\delta^{34}S_{SO4}$ value

of 12.5‰ (Turchyn et al., 2013), the median shift in $\delta^{34}S_{SO4}$ due to this spring contribution would be less than ~4.5‰. The ^{34}S-enriched signal of this input would cause an increase in $\delta^{34}S_{SO4}$ near Syabru Besi, while our data clearly show a decrease in $\delta^{34}S_{SO4}$ at the same junction (Fig. 4).

2.5. Precipitation end-member

In our primary inversion 100% of river [Cl^-] is assumed to derive from precipitation. While the amount, distribution, and major ion composition of precipitation in the Himalaya varies widely, when compared with seawater the dissolved chemistry tends to be enriched in cations relative to Cl^- (Fig S5; Handa, 1968; Galy and France-Lanord, 1999; Bhatt et al., 2000; Andermann et al., 2011; Balestrini et al., 2014; Panthi et al., 2015). This addition of cations to precipitation occurs through incorporation of terrestrial dust (Sequeira and Kelkar, 1978). The uncertainty of our precipitation end-member captures the range of observed compositions, including some level of seasonal variability due to changes in atmospheric circulation (Shrestha et al., 2002). Overall, the inversion-constrained precipitation end-member generally agrees with observations, although reaches slightly higher values of Mg^{2+}/Σ^+ and Cl^-/Σ^+ than are observed (Fig S5).

Except for three samples, attributing 100% of river [Cl^-] to precipitation entails sourcing 3% to 54% of the sum of cations in solution. Although the latter portion of this range may seem high, this magnitude of meteoric input is consistent with prior research. For example, Galy and France-Lanord (1999) report that >65% of total dissolved solids in small high-latitude silicate catchments derive from precipitation, Harris et al. (1998) cite Sarin et al. (1989) in writing that 29±7% of Na^+ is derived through atmospheric deposition in highland rivers, and recent work attributed >50% of Na^+ in streams from the Eastern Himalaya to precipitation, evaporites, and hot springs (Hren et al.,

2007). The most direct comparison comes from West et al. (2002), who calculated that 17% to 61% of the cation flux in small Himalayan catchments is due to atmospheric deposition. That analysis included a re-evaluation of data from the Lirung catchment originally reported in Bhatt et al. (2000), which differed from most other catchments in the West et al. (2002) analysis by showing only 2.3% of [Ca^{2+}] derived from atmospheric deposition (Bhatt et al., 2000; West et al., 2002). For their analysis, West et al. (2002) corrected for Cl^- inputs using snow samples from Yala glacier. However, these samples varied in their Ca^{2+}/Cl^- ratios between 0.1 and 2.4. In part, this large range in Ca^{2+}/Cl^- reflects that the samples were collected at differing depths and in differing seasons, and thus reflect a heterogeneous material averaged over different durations of time (Bhatt et al., 2000). Using rainwater measurements (Table 1) as opposed to snow, a forward model finds that 2-13% of the Ca^{2+} and 7-29% of the Na^+ in the Bhatt et al. (2000) Lirung data is attributable to atmospheric inputs. Similarly, our full inversion model finds 1-9% of the Ca^{2+} and 5-28% of Na^+ in that data is attributable to atmospheric inputs. These updated calculations bring the magnitude of atmospheric deposition in line with expectations from the other catchments in West et al. (2002).

2.6. Anthropogenic impacts on river chemistry

All sample sites in this study are located within 100 km of Kathmandu, and LNS-4 and LNS-3 are only approximately 30 km away from the city. Because prior research has identified ubiquitous SO_4^{2-} pollution in rivers globally (Berner, 1971), even in relatively isolated systems, either global anthropogenic inputs or local urban pollution could influence our observations. At the local scale, Collins and Jenkins (1996) identified significant impacts from agricultural activity on the dissolved chemistry of rivers within the Middle Mountains approximately 10 km north of Kathmandu; soil

tillage was found to increase weathering rate and the overall ion budget of rivers, but with disproportionate increases in [NO_3^-] and [SO_4^{2-}] due to fertilizer application.

Anthropogenic pollution was previously proposed to be ^{34}S-depleted, but recent research reveals a lack of correlation between river pollution and $\delta^{34}S_{SO4}$ (Burke et al., 2018); our analysis of pollution is thus based on measurements of ion concentrations. The concentration of dissolved ions indicate that pollution has only a minimal impact on our samples (Fig. S6a). The ratios SO_4^{2-}/Σ^+ and SO_4^{2-}/Cl^- generally decrease with elevation, opposite to the trend expected if pollution from SO_4^{2-}-bearing fertilizers were entering the river at sites near Kathmandu. However, changes in SO_4^{2-}/Σ^+ are also influenced by downstream changes in lithology. As a result, these observations can only be considered evidence that pollution, if present, is of secondary importance to downstream changes in chemical weathering.

A second approach to identifying pollution is to consider the ratio of Cl^- to Na^+. Only 7 of our samples have Na^+/Cl^- less than 1.1, which was previously used as a threshold value for pollution (Burke et al., 2018). These 7 samples are distributed across sampling sites and were all collected in July, August, and September. Because these samples are unrelated with proximity to Kathmandu, they do not clearly indicate anthropogenic inputs.

Conversely, river pH measurements do provide tentative evidence of anthropogenic inputs (Fig. S6b). Of the 76 samples with pH measurements, 10 values are lower than 6.5 and 1 sample has a pH lower than 5.5. The samples with low pH values are found in stations LNS-3 through LNS-7, all relatively close to Kathmandu (Fig. 1). These acidic samples span the seasonal cycle but are

concentrated during the pre-monsoon season. The lack of low pH values in other stations and seasons may be attributed to sampling bias because sites upstream of LNS-7 each have only a single pH measurement, all from October, and all of which are circumneutral. The low pH values thus potentially indicate either a seasonal pollutant dominant in the pre-monsoon season, or alternatively a constant input of pollution diluted by higher discharge during the monsoon season, and which may or may not be localized to the region near Kathmandu. Because low values of SO_4^{2-}/Σ^+ argue against the addition of SO_4^{2-}-bearing fertilizer, the low-pH samples may indicate the formation of HNO_3 following oxidation of anthropogenic NH_4^+. It is notably that some of the highest measured [NH_4^+] values are found in the Langtang headwaters (Fig. S6c), with several lower values closer to Kathmandu, and which likely also reflects the grazing activities of livestock near the Langtang headwaters. We are unable to interpret original [NO_3^-] (Fig. S6d) determinations or measure [NO_3^-] in the sample bottles now due to artifacts of sample storage (Appendix 1).

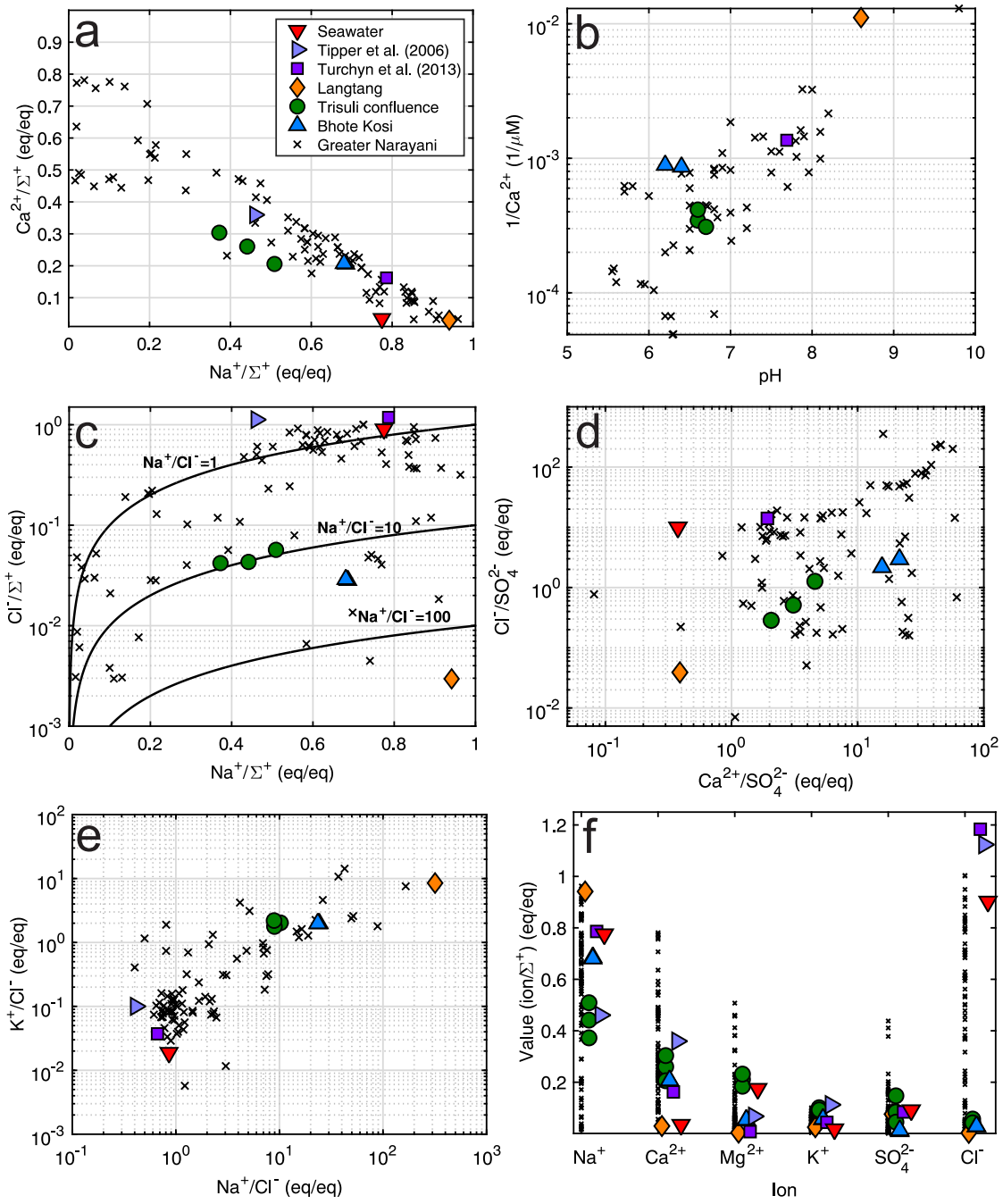

Fig. S4: Dissolved chemistry of springs in the Narayani River system. (a) Ca^{2+}/Σ^{+} against Na^{+}/Σ^{+} suggests mixing between a seawater-like end-member and a low-Na^{+}/Σ^{+} end-member similar to Himalayan river water. (b) The Ca^{2+} dynamic is complicated by an apparent relationship with pH, likely resulting from calcite dissolution at low pH and calcite precipitation at high pH. (c) Cl^{-}/Σ^{+} against Na^{+}/Σ^{+} shows that most data plot near a Na^{+}/Cl^{-} of 1, consistent with seawater, but this observation may simply reflect the abundance of data from the Marsyandi River. Springs near the Langtang-Trisuli Rivers have lower Na^{+}/Cl^{-} ratios. (d) Cl^{-}/SO_4^{2-} against Ca^{2+}/SO_4^{2-} is suggestive of mixing, but at lower Cl^{-} than implied by a seawater end-member. (e) K^{+}/Cl^{-} and Na^{+}/Cl^{-} again show evidence for mixing, but in the opposite sense as Ca^{2+}/Σ^{+} against Na^{+}/Σ^{+} (compare relative position of seawater and the Langtang spring). (f) Summary of data on spring chemistry.

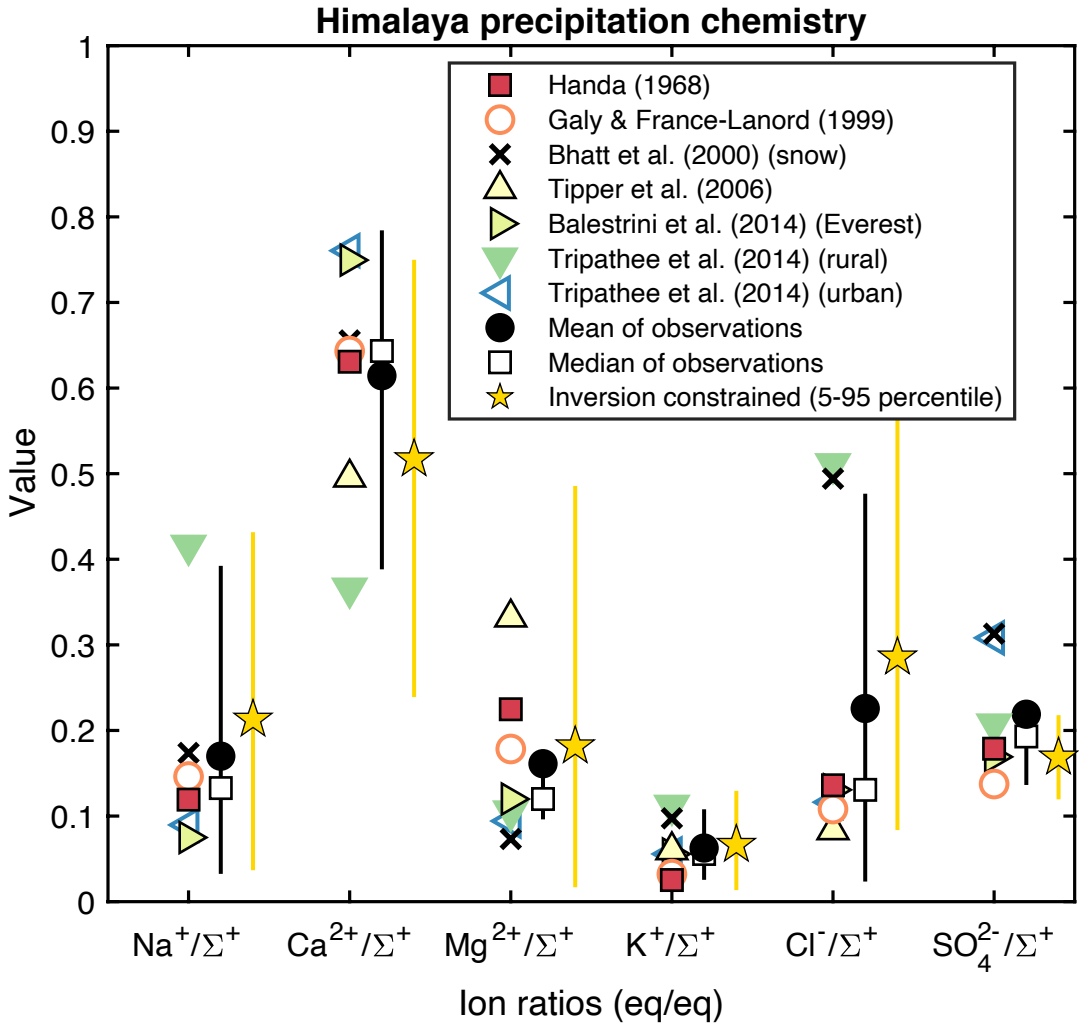

Fig. S5: Major ions chemistry normalized to the sum of cations ($[Ca^{2+}] + [Mg^{2+}] + [Na^{+}] + [K^{+}]$ in units of charge equivalents) in Himalayan precipitation. Precipitation tends to be enriched in Ca^{2+} and depleted in Cl^{-} relative to seawater. The mean (black circles) and median (white squares) of observations are shown, as is the inversion-constrained range of precipitation chemistry (yellow star and line). Data are from Handa (1968), Galy and France-Lanord (1999), Bhatt et al. (2000), Tipper et al. (2006), Balestrini et al. (2014), and Tripathee et al. (2014).

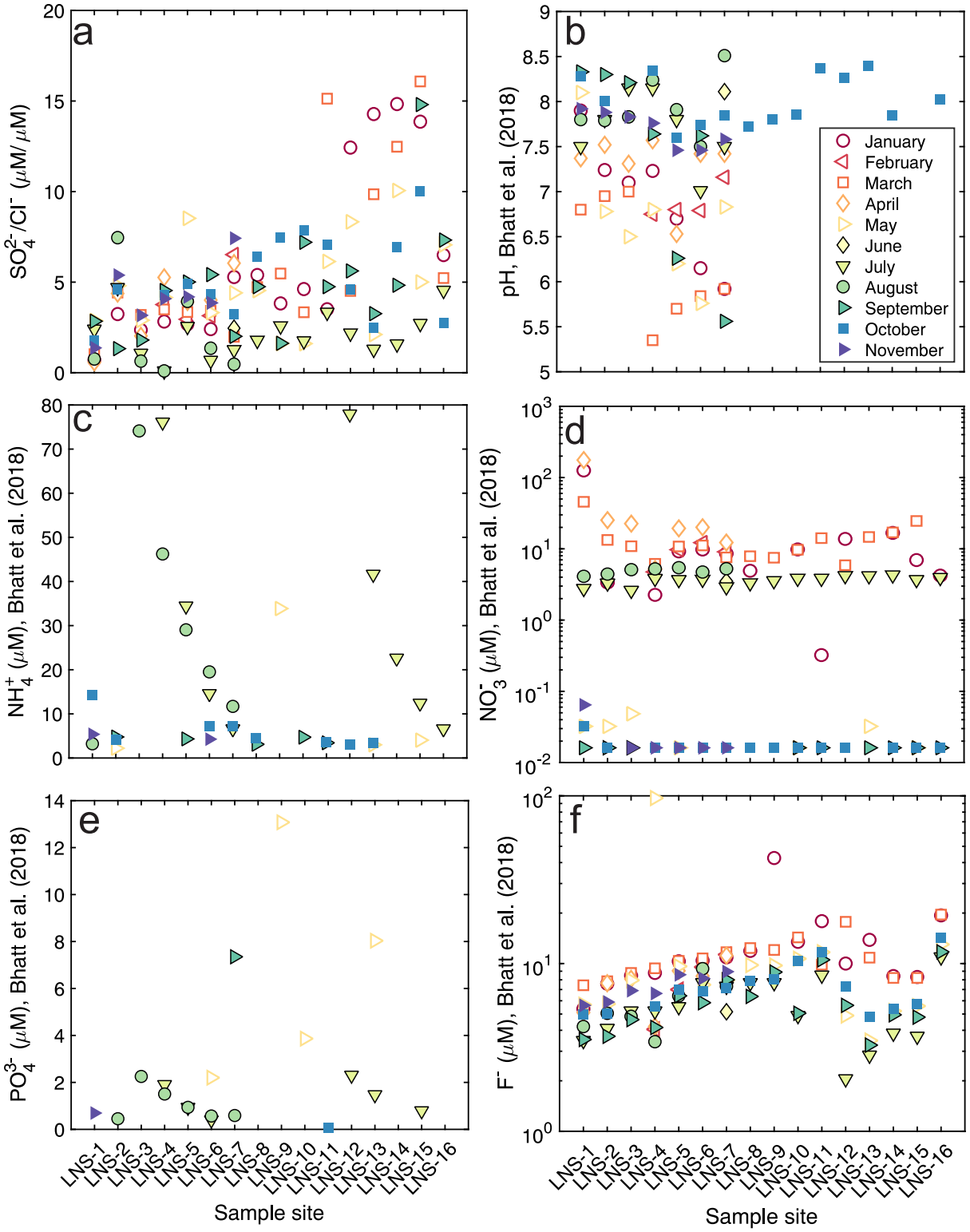

Fig. S6: (a) SO_4^{2-}/Cl^- measurements (Caltech dataset) decline moving downstream. (b) pH of water samples, as reported in Bhatt et al. (2018). The lowest pH values tend to occur during the pre-monsoon season but may p artly reflect a sampling bias. (c) NH_4^+, (d) NO_3^-, (e) PO_4^{3-}, (f) F^- measurements (data from Bhatt et al. (2018)), are not clearly related with proximity to Kathmandu. Seasonal signals in (c)-(f) may reflect measurement artifacts (Appendix 1).

Appendix 3: Extended data figures
3.1 Discharge curves

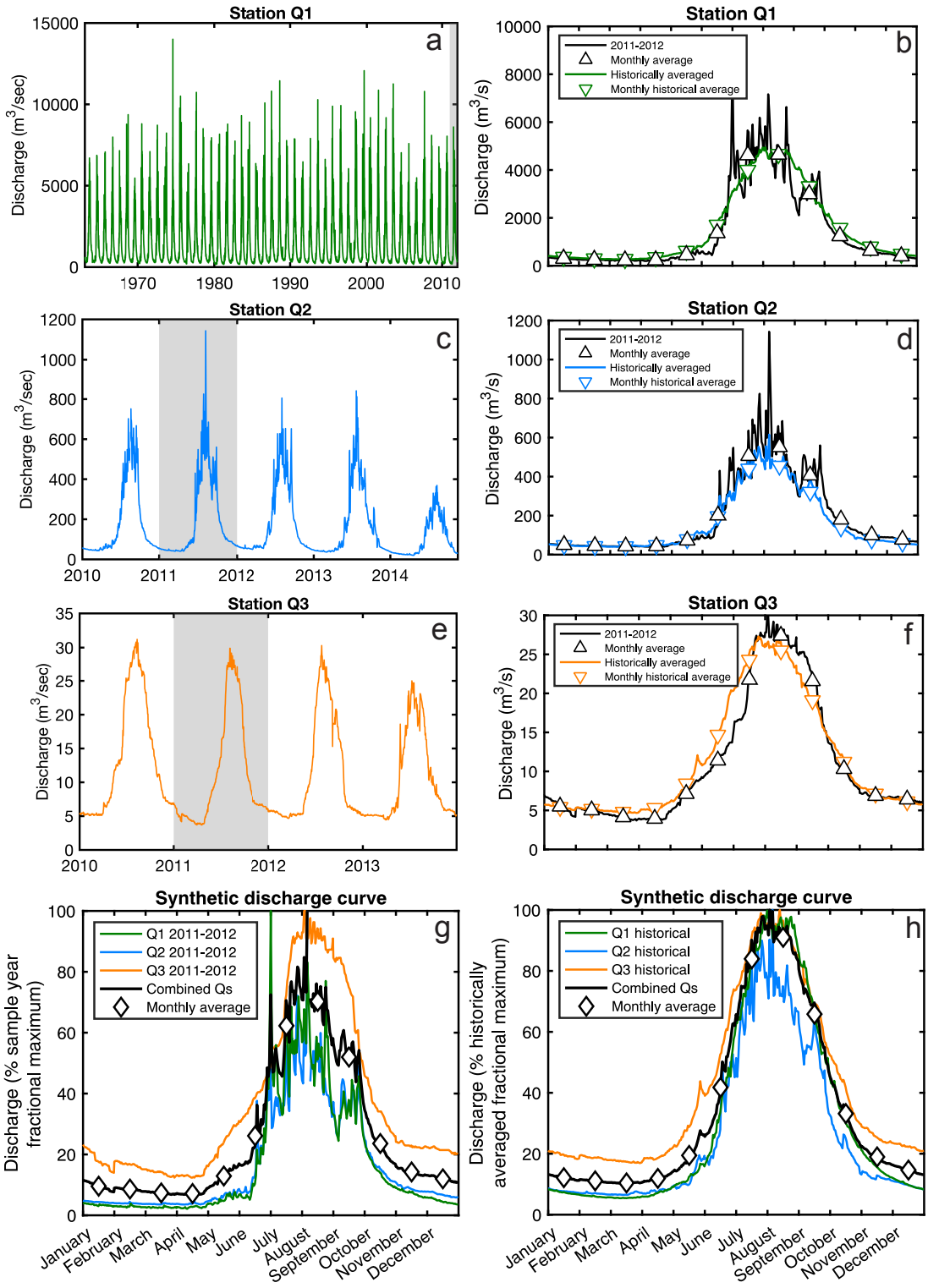

Fig. S7: Derivation of the fractional discharge curve used for sample regression. (a, c, e) Data from the three gauging stations (Fig. 1). (b, d, f) 2011 data, historical average, and monthly averages. (g) The derived fractional discharge curves for 2011 data or (h) for all historical data.

3.2. Impacts of secondary carbonate precipitation

A river dominated by $CaCO_3$ weathering with limited FeS_2 oxidation would be expected to have high Ca^{2+}/Σ^+ and low SO_4^{2-}/Σ^+ ratios (Fig. S8, red square). Precipitation of $CaCO_3$ would decrease Ca^{2+}/Σ^+ and bias the interpretation to lower fractions of carbonate weathering (Fig. S8, blue diamond). It would also increase SO_4^{2-}/Σ^+, making observed SO_4^{2-}/Σ^+ lower than the gross H_2SO_4-driven weathering fraction. Furthermore, the shift in Ca^{2+}/Σ^+ would alter the inversion-constrained range of end-member SO_4^{2-}/Σ^+. However, because the formation of $CaCO_3$ consumes Ca^{2+} and sources H^+, observed SO_4^{2-}/Σ^+ remains an accurate reflection of the net weathering driven by H_2SO_4. The magnitude of these effects depends on the relative abundance of Ca^{2+}, SO_4^{2-}, and the other major ions. Using the median values of our samples and assuming 50% of Ca^{2+} was removed as $CaCO_3$ (Bickle et al., 2015) the absolute shifts in Ca^{2+}/Σ^+ and SO_4^{2-}/Σ^+ are estimated to be ~10%.

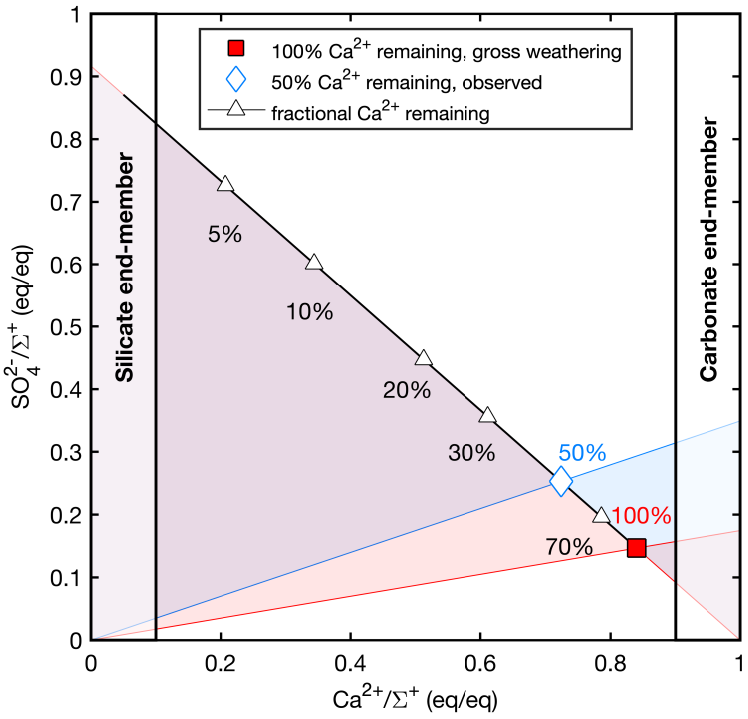

Fig. S8: Impact of secondary carbonate precipitation on dissolved chemistry. Labeled percentages are the fraction of $[Ca^{2+}]$ remaining in solution. This calculation uses approximations to the median observations from this study ($[Na^+]_{median}+[K^+]_{median}+[Mg^{2+}]_{median} \sim 240$ eq., $[SO_4^{2-}]_{median} \sim 220$ eq.), and assumes 50% of Ca^{2+} was removed as $CaCO_3$ prior to our observation ($[Ca^{2+}]_{median} \sim 630$ eq.).

3.3 Sulfur isotope mixing diagrams

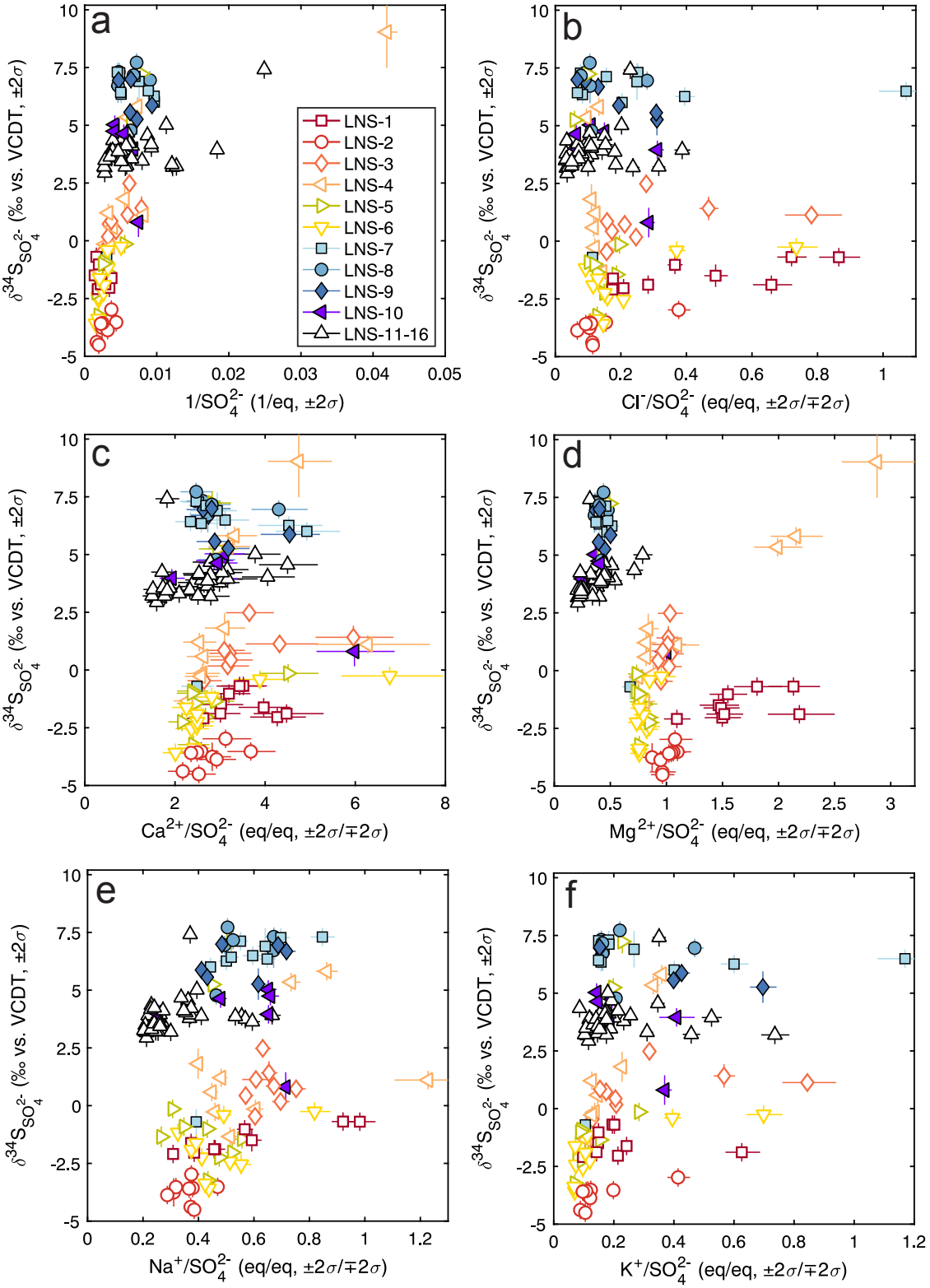

Fig. S9: Sulfur isotope mixing diagrams. Measured $\delta^{34}S_{SO4}$ against (a) $1/SO_4^{2-}$, (b) Cl^-/SO_4^{2-}, (c) Ca^{2+}/SO_4^{2-}, (d) Mg^{2+}/SO_4^{2-}, (e) Na^+/SO_4^{2-}, and (f) K^+/SO_4^{2-}. The lack of coherent relationships argues against simple two end-member mixing as an explanation for observed $\delta^{34}S_{SO4}$ variability.